

# Building Flexible Machine Learning Models for Scientific Computing at Scale

Tianyu Chen<sup>1</sup> Haoyi Zhou<sup>1</sup> Ying Li<sup>2</sup> Hao Wang<sup>2</sup> Chonghan Gao<sup>1</sup> Shanghang Zhang<sup>2</sup> Jianxin Li<sup>1</sup>

## Abstract

Foundation models have revolutionized knowledge acquisition across domains, and our study introduces OmniArch, a paradigm-shifting approach designed for building foundation models in multi-physics scientific computing. OmniArch’s pre-training involves a versatile pipeline that processes multi-physics spatio-temporal data, casting forward problem learning into scalable auto-regressive tasks, while our novel Physics-Informed Reinforcement Learning (PIRL) technique during fine-tuning ensures alignment with physical laws. Pre-trained on the comprehensive PDEBench dataset, OmniArch not only sets new performance benchmarks for 1D, 2D and 3D PDEs but also demonstrates exceptional adaptability to new physics via few-shot and zero-shot learning approaches. The model’s representations further extend to inverse problem-solving, highlighting the transformative potential of AI-enabled Scientific Computing (AI4SC) foundation models for engineering applications and physics discovery.

## 1. Introduction

Developing robust neural surrogate models for temporal partial differential equations (PDEs) is crucial for a variety of scientific and engineering applications, including aircraft design, weather forecasting, and semiconductor manufacturing (Allen et al., 2022; Pathak et al., 2022). These PDEs describe spatial-temporal dynamic systems that are foundational to these industries. Traditional scientific computing methods, such as Finite Element Methods (FEM) and Finite Volume Methods (FVM) (Oden, 1989), require extensive handcrafted coding and are computationally intensive, even on state-of-the-art High-Performance Computing (HPC) clusters. To expedite PDE solving, pioneers have explored the construction of neural operators that learn mappings between function spaces, offering the potential to generalize

<sup>1</sup>Beihang University <sup>2</sup>Peking University. Correspondence to: Jianxin Li <lijx@buaa.edu.cn>.

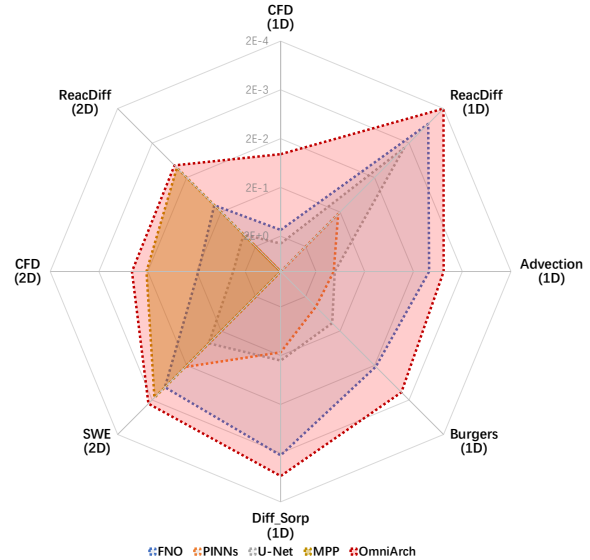


Figure 1: OmniArch achieves state-of-the-art performance on a broad range of tasks except 3D compared with other task-specific models.

across different discretizations. For the requisite precision, neural operators are often enhanced with physics-informed normalization techniques, such as customized loss functions derived from the governing physical equations (Raissi et al., 2019).

The primary limitation of neural operator methods is their case-specific design, which restricts application scope and hinders broad transferability across diverse physical systems. Recent efforts aim to enhance the transferability of neural operators by developing foundational models that leverage advancements in learning strategies, architectural design, and data curation. In terms of learning, the “pre-train and fine-tune” paradigm, proven effective for Fourier Neural Operator (FNO) models (Subramanian et al., 2023), has been adapted to PDE contexts. Additionally, Lie group-based self-supervised learning (Lie-SSL) (Mialon et al., 2023) introduces physics-constrained transformations for PDEs, primarily addressing inverse problems. Architecturally, innovations like ICON LM (Yang et al., 2023b) and PITT (Lorsung et al., 2023) incorporate language model principles to enhance neural operator learning, enabling generalization through equation captions. The Factformer

(Li et al., 2023) introduces a scalable transformer for multi-dimensional PDE data, with the Multi-Physics Pre-training (MPP) (McCabe et al., 2023) further extending this approach to 2D data pre-training. From a data-centric viewpoint, resources such as PDEBench (Takamoto et al., 2022) and PDEArena (Gupta & Brandstetter, 2022) offer well-structured datasets that facilitate both pre-training and the establishment of rigorous benchmarks.

Recent studies have attributed the efficacy of transformers in foundation models to their minimal inductive biases, which is particularly advantageous for complex reasoning tasks (Bhojanapalli et al., 2021; Wei et al., 2022). Traditional surrogate models, often constrained by finite element method (FEM) frameworks, require grid and time inputs, imposing significant inductive biases that limit their generalizability and flexibility for SciML applications. To address this, we propose a grid-independent approach that learns from dynamic observation windows, a strategy that is mesh-free and capable of capturing long-term patterns. Instead of explicitly input the grid and time information, we enforce the model to learn from the derivatives of the input sequence. This design enables a unified representation of diverse PDE systems. Our experiments confirm that this approach not only improves temporal dynamics comprehension but also enhances model transferability.

In this work, we study how to frame the foundation model learning paradigm for Scientific Computing tasks w.r.t PDEs, namely OmniArch. For the pre-training stage, we define a flexible pipeline to deal with multiple-physics spatial-temporal data and convert the forward problem learning into the popular auto-regressive tasks which is friendly to be scaled up. To do that, we introduce the "axis numerical encoding" and "channel-wise tokenize" techniques to convert the temporal PDEs into sequence of tokens which could be handled by current transformer blocks. In the fine-tuning stage, inspired by the reinforcement learning with human feedback (RLHF) techniques, we train a physics-informed scorer to guide the prediction of generator, which in further align the predictions with expert understanding of physics laws.

We release three versions of our model, covering the 1D, 2D and 3D PDEs. We test the performance of our models in the 9 Types of PDEs on the PDEBench and find we all got SOTA performance as illustrated in Figure 1, for the CFD related tasks, the nRMSE drops down to one or two order of magnitudes. In addition, we observe some emergent ability of our models, such as zero-shot to other PDE systems or inverse inference the initial state. We also find the representations produced by OmniArch could easily be adapted to other tasks like the inverse problem. For the efficient inference, we investigate the jumping context technique which could balance the cost of inference time

with precision of prediction.

Our key contributions and findings include:

1. We introduce OmniArch, a mesh-free, foundation model framework for PDEs that Learn from dynamic observational windows, enabling unified handling of diverse spatial-temporal data and capturing of extended temporal patterns without traditional grid reliance.
2. Utilizing auto-regressive pre-training with "axis numerical encoding", coupled with fine-tuning through a physics-informed scorer based on RLHF, OmniArch achieves state-of-art performance across various PDE benchmarks.
3. The model exhibits zero-shot learning for novel PDE systems and facilitates inverse problem-solving, with a 'dynamic prompting' technique to balance inference speed and prediction accuracy effectively.

## 2. Related Works

**Pretrained Foundation Models:** Pretrained Foundation Models (PFMs) (Bommasani et al., 2021) have emerged as pivotal elements in the field of Artificial Intelligence (AI), particularly in the big data milieu. They serve as the bedrock for a multitude of downstream tasks across diverse data modalities (Zhou et al., 2023). A foundation model encapsulates a broader spectrum of models and functionalities, offering an effective parameter initialization for an extensive array of downstream applications, including but not limited to models like BERT (Devlin et al., 2018) and GPT (Brown et al., 2020; Radford et al., 2019; 2018). The Transformer architecture (Vaswani et al., 2017) plays a critical role within PFMs across various domains. Its ability to address long-range dependencies in sequential input data (Lin et al., 2022; Wen et al., 2022) renders it exceptionally adept at learning spatiotemporal relationships inherent in PDEs (Blechsmidt & Ernst, 2021; Beck et al., 2020). Our model, which is based on the Transformer architecture and has been trained on a substantial corpus of data, establishes itself as a foundational model adept at tackling physical systems governed by PDEs.

**Learned PDE Solvers:** Recently, the application of deep learning architectures for solving PDEs has been a focal point of research (Lu et al., 2021b; Karniadakis et al., 2021). Physics-informed methods (Raissi et al., 2019; Sun et al., 2020; Sirignano & Spiliopoulos, 2018) leverage PDE supervision to approximate solutions across aggregated space-time domains, offering accuracy and a generally mesh-independent approach. However, they necessitate retraining for different PDE instances. DeepONet (Lu et al., 2021a) stands as a trailblazer in the realm of neural operators, ingeniously incorporating system-specific prior knowledge

(Wang et al., 2021). The Fourier Neural Operator (FNO) (Li et al., 2020) and its subsequent iterations (Li et al., 2021; Guibas et al., 2021; Tran et al., 2021) have demonstrated their efficacy in a variety of contexts. Building on the momentum of attention mechanisms (Vaswani et al., 2017), numerous studies (Geneva & Zabarar, 2022; Kissas et al., 2022; Han et al., 2022) have utilized attention to model and simulate physical phenomena. The Galerkin Transformer (Cao, 2021), for instance, employs attention layers to discern the underlying structures and patterns within the spatial domain of PDEs. These methodologies have robustly validated the potential of neural networks to approximate solution operators. Nevertheless, they predominantly focus on approximating solutions to specific equations or operators, and thus require retraining for each new problem or set of equations.

In contrast, In-Context Operator Networks (ICON) (Yang et al., 2023a) aim to concurrently learn operators from the provided data and apply them to novel queries during inference. Meanwhile, Multiple Physics Pretraining (MPP) (McCabe et al., 2023) involves training expansive surrogate models capable of predicting the dynamics of various heterogeneous physical systems. This is achieved by extracting features with broad applicability across diverse physical scenarios. However, a lack of comprehensive data can hinder these models from discerning the fundamental connections between different PDEs, limiting their ability to tackle cross-dimensional PDE challenges. Our proposed model, which is trained on a voluminous dataset, is designed to address these limitations. It is capable of resolving problems involving different equations across multiple dimensions and exhibits remarkable adaptability to new domains within the physical sciences.

### 3. Background

**Notation:** Let  $\mathcal{E}$  denote the set of parameterized partial differential equations (PDEs) describing a spatiotemporal dynamical system  $\mathcal{S}$ . We represent the snapshots of the observed physical fields within the system by  $\mathcal{P}$ . A continuous state variable for system  $\mathcal{S}$  is defined as  $u^S(x, t) : [0, L_S] \times [0, \infty) \rightarrow \mathbb{R}$ , where  $[0, L_S]$  is the spatial domain and  $[0, \infty)$  is the temporal domain. We discretize the system uniformly in space and time with resolutions  $N_S$  and  $T_S$ , respectively. A snapshot  $u_i^S \in \mathbb{R}^{N_S}$  represents the values of the state variable  $u^S$  at all  $N_S$  spatial discretization points at time  $t$ .

**Forward Problem:** Given the equations  $\mathcal{E}$ , the objective is to find the solution function  $\mathbf{u}^S(x, t)$ , which predicts the state of the dynamical system  $\mathcal{S}$  at any spatiotemporal coordinate  $(x, t)$ .

**Inverse Problem:** Given a set of partial PDEs  $\tilde{\mathcal{E}}$  or, in some

cases, no explicit PDE information, along with observations comprising  $T_S$  snapshots  $U_t^S = [u_1^S, u_2^S, \dots, u_i^S]$ , the goal is to infer the missing components of the PDEs (such as boundary conditions, hyperparameters, or the form of the equations) or to reconstruct the complete PDE  $\hat{\mathcal{E}}$ .

## 4. Method

### 4.1. Flexible Multiple Physics Pretraining

Natural systems involve various types of physical phenomena operating at different spatial and temporal scale. For example, almost all practical problems in fluid dynamics involve the interaction between a gas and/or a liquid with a solid object, and include a range of associated physics including heat transfer, particle transport, erosion, deposition, flow-induced stress, combustion and chemical reaction. A multiple-physics environment is defined by coupled processes or systems involving more than one simultaneously occurring physical fields or phenomena. Such an environment is typically described by multiple partial differential equations (PDEs), and tightly coupled such that solving them presents significant challenges with nonlinearities and time-stepping. For Surrogation models to be accurate and useful, they must support multiple physics and multiple scales (spatial and temporal).

As illustrated in Figure 2, We propose an innovative pipeline for Multiple Physics Pre-training that effectively handles multi-dimensional Partial Differential Equation (PDE) Systems. The framework is composed of a tokenization and encoding scheme, a state representation strategy for multi-channel PDEs, an auto-regressive training mechanism, and a specialized optimization criterion. Here, we delineate each component in detail, supplemented with mathematical formalizations.

**Tokenization and Axis Encoding:** The foundation of our approach is the transformation of continuous physical fields into a discrete tokenized format suitable for deep learning models and scale up. Let  $\mathcal{F}$  denotes a physical field, which is a function of space  $\mathbf{x}$  and time  $t$ , such that  $\mathcal{F} : \mathbf{x}, t \mapsto \mathbb{R}^C$ , where  $C$  represents the number of channels. We define an axis encoder  $E : \mathbb{R}^M \mapsto \mathbb{R}^H$ , where  $M$  is the dimensionality for the physical field (e.g., 2 for 2D fields, 3 for 3D fields), and  $H$  is the fixed hidden size. The encoder transforms the spatial dimensions into a hidden representation:

$$\mathbf{h}_{\mathbf{x},t} = E(\mathcal{F}(\mathbf{x}, t)) \quad (1)$$

The hidden vectors  $\mathbf{h}_{\mathbf{x},t}$  are subsequently flattened to form the input embeddings, analogous to the procedure in Xval (Golkar et al., 2023).

**Channel-wise State Representation:** For a PDE system with multiple channels, we represent the state at a given timestep

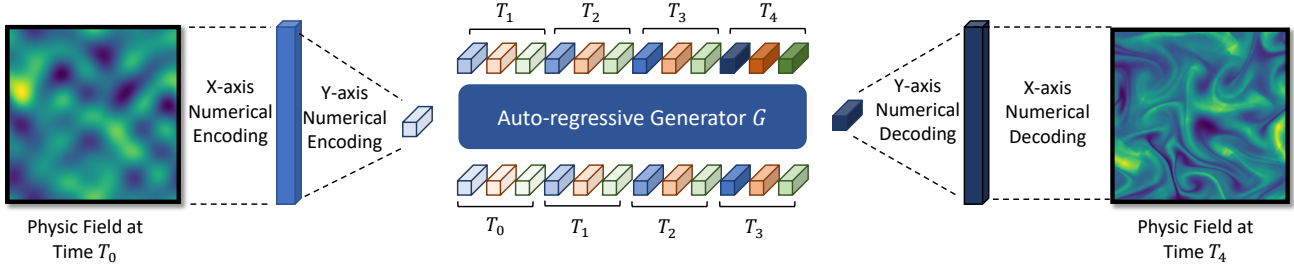


Figure 2: The OmniArch pretraining pipeline, exemplified here for 2D physical fields, is a flexible framework capable of accommodating 1D, 2D, and 3D tasks. The process begins with a lightweight numerical encoder that discretizes the continuous physical field into a sequence of tokens. These tokens are then processed through an auto-regressive model that predicts subsequent state representations. The figure illustrates the transformation from spatial-temporal data to an encoded token sequence, followed by the predictive modeling and the final decoding back to the physical domain.

$t$  as a sequence of grouped tokens  $\mathbf{T}_t$ , where each group includes  $C$  tokens. This allows for the expression of inter-channel and intra-channel relationships and dependencies on previous timesteps:

$$\mathbf{T}_t = [\mathbf{h}_{1,t}; \mathbf{h}_{2,t}; \dots; \mathbf{h}_{C,t}] \quad (2)$$

This matrix facilitates attention mechanisms within and across channels, enhancing the model’s ability to capture complex dynamics, as inspired by the Decision Transformer (Chen et al., 2021).

**Auto-regressive Training with Shift-Right:** Our auto-regressive model is trained using a shift-right technique, which ensures causality in the prediction sequence. For a sequence of states  $\mathbf{T}_{1:T}$ , the model predicts the next state token  $\hat{\mathbf{T}}_{t+1}$  based on the previous states. Formally, the model generates predictions as  $\hat{\mathbf{T}}_{t+1} = G(\mathbf{T}_{1:t})$ .

**Optimization via Batch-wise nRMSE:** Considering the numerical distribution variance between different PDE systems, we apply the batch-wise Normalization Root Mean Square Error (nRMSE) (McCabe et al., 2023) as the loss function. Let  $\hat{\mathcal{F}}$  denote the predicted physical field, the nRMSE for a batch  $B$  is given by:

$$\text{nRMSE}(B) = \frac{1}{|B|} \sqrt{\sum_{(\mathbf{x},t) \in B} \left( \frac{\mathcal{F}(\mathbf{x},t) - \hat{\mathcal{F}}(\mathbf{x},t)}{\sigma_{\mathcal{F}}} \right)^2} \quad (3)$$

where  $\sigma_{\mathcal{F}}$  is the standard deviation of the true physical field values over the batch. The training process involves the iterative minimization of this metric across batches.

**Decoder with Axis Numerical Embedding:** In the decoding phase, we utilize the inverse of the axis encoding function,  $E^{-1} : \mathbb{R}^H \mapsto \mathbb{R}^D$ , to reconstruct the physical

field from the hidden representation. The decoder outputs a physical field  $\hat{\mathcal{F}}$  corresponding to the predicted tokens:

$$\hat{\mathcal{F}}(\mathbf{x},t) = E^{-1}(\hat{\mathbf{h}}_{\mathbf{x},t}) \quad (4)$$

This ensures that the model’s output is mapped back to the original physical field dimensions, facilitating direct comparison with the ground truth data. Our pretraining strategy is designed to be robust and generalizable, enabling the model to learn from and adapt to a diverse array of PDE systems.

## 4.2. Physics-informed Reinforcement Learning

Let  $\mathcal{D}$  be the dataset containing pairs of physical field data and their corresponding weakly annotated PDE captions, i.e.,  $\mathcal{D} = (\mathbf{x}_i, \mathbf{t}_i)_{i=1}^N$ , where  $\mathbf{x}_i$  represents a frame of physical field data, and  $\mathbf{t}_i$  is the textual equation, boundary conditions, and other related annotations in natural language.

**Physics-Informed Scorer Model S:** Train a CLIP-style model  $S$  that takes a pair of physical field data  $\mathbf{x}$  and its corresponding PDE caption  $\mathbf{t}$ , and outputs a similarity score  $s \in \mathbb{R}$  indicating the match between the data and the textual information:  $S(\mathbf{x}, \mathbf{t}; \theta_S) \rightarrow s$ , where  $(\theta_S)$  represents the parameters of the scorer model  $S$ .

**Pretrained Model G:** Let  $G$  be a model that takes a sequence of recent time steps of physical fields  $\mathbf{X}_{(0:t)} = \mathbf{x}_0, \mathbf{x}_{\delta_t}, \dots, \mathbf{x}_t$  as input and predicts the physical field  $\hat{\mathbf{x}}_{t+1}$  at the next time step:  $G(\mathbf{X}_{(0:t)}; \theta_G) \rightarrow \hat{\mathbf{x}}_{t+1}$ , where  $\theta_G$  represents the parameters of the generative model  $G$ . In this work, we take the pre-trained OmniArch as  $G$ .

**Fine-Tuning with Physics-Informed Rewards:** During fine-tuning, for each input sequence  $\mathbf{X}_{(0:t)}$  and its corresponding PDE caption  $\mathbf{t}$ , the model  $G$  generates a prediction  $\hat{\mathbf{x}}_t$ . The scorer model  $S$  then evaluates this prediction against the PDE caption, providing a reward



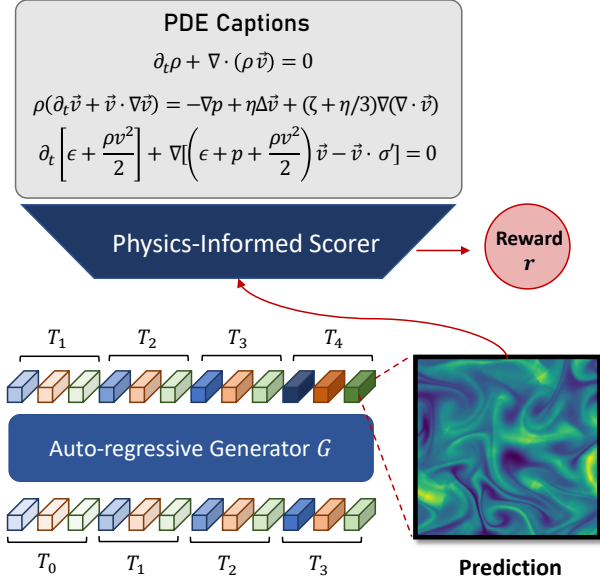


Figure 3: Illustration of the Physics-Informed Reinforcement Learning (PIRL) methodology. The PIRL method utilizes a Physics-Informed Scorer to evaluate predictions against PDEs and associated conditions. Higher rewards are given for predictions that align with physical laws, guiding the model towards physically plausible solutions.

$r : r = S(\hat{\mathbf{x}}_{t+1}, \mathbf{t}; \theta_S)$ . This reward signal is used to update the parameters of  $G$  using reinforcement learning techniques, typically by maximizing the expected reward:

$$\theta_G^* = \arg \max_{\theta_G} \mathbb{E}(\mathbf{X}_{(0:t)}), \mathbf{t} \sim \mathcal{D}[r] \quad (5)$$

This process iteratively aligns the predictions of model  $G$  with the physical laws described by the PDE captions.

## 5. Experiments

First, we report our main results of forward problems by pretraining the model on the PDEBench. In the following sections, we explore the inverse problem, the impact of fine-tuning, the zero-shot generalization of parameters, equation, temperally and spatially.

### 5.1. Data and Setup

**Pre-training Stage:** We structured the PDEBench data into distinct training, validation, and testing subsets. For one-dimensional (1D) PDEs, the training dataset comprises a selection from the 1D\_CFD, ReacDiff, Advection, Burgers, and diff-sorp datasets. From these, we reserve a random 10% sample of trajectories as the in-domain test set for each respective PDE equation. The Shock Tube Equation is designated as the out-of-domain test set. Additionally, the test portions of the reacdiff and diff-sorp datasets are

utilized as part of the test set.

In the two-dimensional (2D) PDE case, we allocate 90% of trajectories from the CFD, diff-react, NSincom, and shallow water datasets for training. The remaining 10% form the in-domain test set. The Shock Tube, Kelvin-Helmholtz instability (KH), and Tolman-Oppenheimer-Volkoff (TOV) scenarios are included as out-of-domain test sets.

For three-dimensional (3D) PDEs, 90% of trajectories from the 3D\_CFD dataset are utilized for training, with the remaining 10% serving as the in-domain test set. The complete datasets for blastwave and turbulence simulations are used as out-of-domain test sets. The Details of our pre-training dataset could be found in Table 1.

Table 1: Data Statistics for OmniArch Pre-training

Dataset	#Train	#Validation	#Test	$N_t$	$N_s$
1D	378000	42000	28	81	1024
2D	42300	300	8	21	128
3D	630	70	6	21	64

To fully utilize the ecology of foundation models, we use the LLaMA Model (Touvron et al., 2023a;b) as our autoregressive generator  $G$ . For the 2D and 3D tasks, we apply a parallel convolutional encoder with the axis numerical encoder for better high-frequency pattern capturability. For the decoder, we use the sum of logits from both transposed convolutional decoder and the weights-bined inverse axis numerical decoder. More Training Details could be found in Appendix B.

**Implementation of PIRL:** Given the significant imbalance between equation caption data and physical field data, a single equation can yield a multitude of physical field simulations. To augment equation captions effectively, it is crucial to preserve the equation’s solutions and boundaries while adhering to physical laws and exploring a wide array of possible substitutions. To achieve this, we have developed a five-step augmentation pipeline: *Equation Rewriting*, *Form Transformation*, *Linear Combination*, *Symbol Substitution*, and *Physical Checking*:

- **Equation Rewriting:** We apply mathematical identities to modify the equation, ensuring the core properties remain intact.
- **Form Transformation:** We transform equations between differential and integral forms and employ techniques such as Green’s functions to broaden the equation’s representations.
- **Linear Combination:** For systems of equations, we derive new variants through linear combinations, enriching the dataset without altering the system’s nature.

- **Symbol Substitution:** We systematically swap variables with alternative symbols, such as replacing  $x$  with  $\xi$ , to maintain consistency and avoid ambiguity.
- **Physical Checking:** A panel of GPT-4-based experts evaluates the augmented equations, filtering out those that do not align with physical principles.

Leveraging the first four steps, we generate 200 augmented instances per equation type. Subsequently, during the Physical Checking phase, we select the top 50% of these examples based on quality for pre-training. Representative samples of the augmented examples are available in Appendix A.2.

In our architecture, the physics-informed Scorer is bifurcated into a text encoder and a physics encoder. The text encoder leverages the pre-trained albert-math model (Reusch et al., 2022), which is adept at processing LaTeX-encoded PDE captions due to its extensive training on a large corpus of LaTeX data. For the physics encoder, we implement a streamlined one-channel Vision Transformer (ViT) model tailored to both 1D and 2D PDEs, and we adopt a large-batch contrastive learning approach, akin to the CLIP framework (Radford et al., 2021). Training involves a stochastic sampling strategy where there is a balanced probability (50%) of selecting either the canonical PDE captions—sourced directly from textbooks—or augmented PDE captions, with the latter assumed to bolster the text encoder’s generalization capabilities while retaining critical PDE information in textual form. During the reward phase, the Scorer evaluates the alignment of gold PDE captions with the state of physical fields at each step of the generator G’s decoding process. The resulting rewards are averaged over the temporal dimension and finalized upon the completion of inference.

## 5.2. Baselines

In our experiments, we adopt the benchmarking framework provided by PDEBench (Takamoto et al., 2022) and select three well-established methods for comparative analysis. Furthermore, we have incorporated the Multiple Physics Pretraining (MPP) model into our comparative analysis to address the need for retraining that is inherent to the aforementioned methods when faced with novel sets of conditions.

**Physics-Informed Neural Networks (PINNs) (Raissi et al., 2019)** : PINNs utilize neural networks to solve differential equations by embedding physical laws into a multi-objective optimization framework, minimizing PDE residuals and boundary/initial condition errors (Cuomo et al., 2022).

**U-Net (Ronneberger et al., 2015)** : U-Net, designed for biomedical image segmentation, uses an encoder-decoder

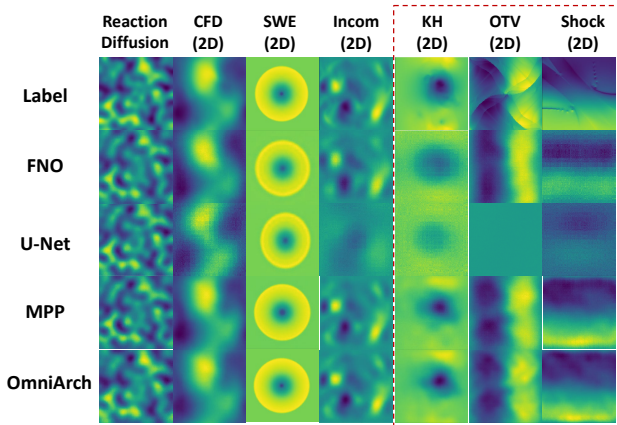


Figure 4: Visualization of 2D PDE Predictions at the Final Time Step. This figure compares the predictive capabilities of FNO, U-Net, and OmniArch, with a focus on zero-shot performance for out-of-domain examples, highlighted within the red dotted-line boxes.

structure for context capture and precise localization (Sidique et al., 2021; Du et al., 2020). We adapt U-Net into 1D and 3D forms to analyze spatiotemporal patterns in physical fields.

**Fourier Neural Operator (FNO) (Li et al., 2020)** : FNO pioneers in learning function-to-solution mappings by parameterizing integral kernels in the Fourier domain, enabling efficient and accurate resolution-invariant neural operators.

**Multiple Physics Pretraining (MPP) (McCabe et al., 2023)** : MPP extends PDEBench’s 2D physics scenarios to learn versatile features for predicting dynamics across various physical systems and comprises pre-training and fine-tuning phases, warranting its inclusion in our comparative analysis.

## 5.3. Results and Analysis

### 5.3.1. PRE-TRAINED MODEL VS TASK-TUNED MODEL

Performance metrics, specifically the normalized Root Mean Square Error (nRMSE) for One-Step Prediction, are presented in Table 2. Notably, pre-trained models such as MPP and OmniArch exhibit performance on par with task-tuned models including FNO, PINNs, and U-Net, even prior to fine-tuning. Subsequent fine-tuning with Physics-Informed Reinforcement Learning (PIRL) yields substantial gains for OmniArch across all tasks, with improvements exceeding 49% for 1D tasks and an average enhancement of 20% for 2D tasks. We posit that this is attributable to the model’s capability to internalize common operators prevalent across diverse physical systems, thereby enhancing its generalizability to various PDE solutions. It is important to note that Physics-Informed Neural Networks (PINNs) are

Table 2: Comparative nRMSE Performance for One-Step Prediction (T+1) Across Various PDEs on PDEBench. The table contrasts case-specific models (FNO, PINNs, U-Net) with multi-physics models (MPP, OmniArch). OmniArch demonstrates superior performance, denoted in bold, with the final column showing the percentage improvement over the best baseline.

PDEs		FNO	PINNs	U-Net	MPP-L	OmniArch	+ PIRL	Lead %
1D	CFD	1.4100	-	2.6700	-	0.0981	<b>0.0392</b>	97.2 ↑
	ReacDiff	0.0005	0.2140	0.0026	-	0.0004	<b>0.0002</b>	64.0 ↑
	Advection	0.0091	0.8130	0.7760	-	0.0081	<b>0.0045</b>	49.9 ↑
	Burgers	0.0174	0.9450	0.3200	-	0.0067	<b>0.0032</b>	81.9 ↑
	Diff_Sorp	0.0017	0.2200	0.1500	-	0.0019	<b>0.0006</b>	62.2 ↑
2D	CFD	0.2060	-	1.0700	0.0178	0.0994	<b>0.0153</b>	14.0 ↑
	SWE	0.0044	0.0170	0.0830	0.0022	0.0031	<b>0.0015</b>	3.32 ↑
	ReacDiff	0.1200	1.6000	0.8400	0.0098	0.0993	<b>0.0084</b>	14.0 ↑
	NS-Incom	0.2574	-	1.1200	-	0.1494	<b>0.0827</b>	67.9 ↑
3D	CFD	0.3050	-	0.6150	-	0.6600	0.5072	66.3 ↓

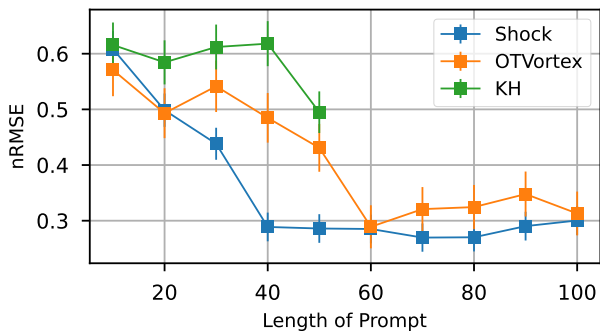


Figure 5: Zero-shot learning nRMSE for T+1 timesteps with varying context lengths.

typically trained per trajectory and struggle with complex equations characteristic of Computational Fluid Dynamics (CFD) or Navier-Stokes incompressible flows (NS-Incom). The MPP Model, while primarily targeting 2D tasks, does not extend its results to 1D or 3D tasks. Our observations also indicate that OmniArch underperforms in 3D task scenarios, which is an area earmarked for future investigation.

### 5.3.2. ZERO-SHOT LEARNING CAPABILITY

Table 3: The Performance on Zero-Shot PDEs.

Methods	Shock	KH	OTVortex
FNO	0.7484	1.0891	0.5946
U-Net	1.6667	0.1677	0.4217
MPP	0.3243	1.3261	0.3025
<b>OmniArch</b>	<b>0.2126</b>	<b>0.5432</b>	<b>0.1718</b>

Our examination of 2D PDE predictions, as shown in Figure 4, reveals that, in contrast to task-tuned models, the

OmniArch model adeptly captures both low- and high-frequency patterns in in-domain PDEs such as Reaction Diffusion, CFD, Shallow Water, and Incompressible NS. Task-tuned models often miss key features, occasionally leading to erroneous representations of the primary physics. For out-of-domain PDEs, delineated by a red-dotted box in the figure, we evaluated the models’ ability to predict unseen PDEs without fine-tuning or parameter adjustment. While task-tuned models consistently failed at this zero-shot learning task, OmniArch successfully predicted essential low-frequency background patterns, though it struggled with high-frequency details. Details on the zero-shot dataset, including shock wave, Kelvin-Helmholtz (KH), and Orszag-Tang Vortex (OTVortex) phenomena, are provided in Appendix A.1.

Furthermore, in Table 3, we report the nRMSE scores, highlighting that all models, except OmniArch, tend to underperform in zero-shot transfer. This suggests that a strict adherence to explicit grid and temporal dependencies may severely restrict the transferability of learned representations to other PDEs. The fixed window size used during pre-training may not be conducive to learning the underlying physics of the observed field states.

In our zero-shot learning evaluation, we explore the minimum number of time steps necessary to formulate accurate neural operators. We also probe the OmniArch model’s ability to generalize to new physics scenarios without parameter adjustments. As indicated in Table 3 and Figure 5, a longer temporal context typically enhances model performance, resulting in lower nRMSE scores across tasks. Notably, our model exhibits impressive zero-shot learning capabilities, maintaining robustness against mesh and temporal interpolation variations, even with fewer than 20 time steps of context.

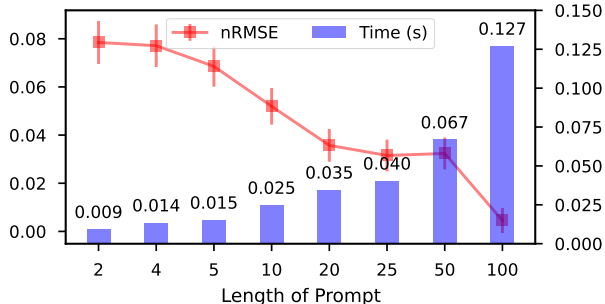


Figure 6: The nRMSE and Inference time with different length of prompt on SWE(2D) Dataset with the OmniArch-L Model.

### 5.3.3. DYNAMIC PROMPT LENGTH FOR EFFICIENT INFERENCE

We examine the trade-off between inference speed and accuracy using dynamic prompt lengths in our model. The goal is to determine whether shorter prompts can accelerate inference times on CPU without significantly sacrificing precision.

Our approach varies the prompt length from 2 tokens (derived from a 50-timestep interval) to 100 tokens (from a 1-timestep interval) to predict physical fields at  $u_{101}$ . As shown in Figure 6, longer prompts yield higher precision with less variance, while shorter prompts can expedite inference by up to 10 times compared to full-length prompts. In particular, our model demonstrates an inherent ability to learn temporal differences from the input sequence, negating the need for explicit time-step inputs.

### 5.3.4. FINE-TUNED FOR INVERSE PROBLEMS

Demonstrating a model’s capability to infer hidden physical parameters from known equations is a critical test of its ability to learn underlying physics. Following the methodology of MPP (McCabe et al., 2023), we evaluate our model on two inverse problems for incompressible Navier-Stokes equations: 1) Forcing Identification, and 2) Buoyancy Determination.

Table 4: RMSE for Parameter Estimation in Inverse Problems.

Methods	Forcing	Buoyancy
<b>MPP</b>	$0.2 \pm 0.008$	$0.78 \pm 0.006$
<b>OmniArch</b>	$0.16 \pm 0.005$	$0.73 \pm 0.012$
<b>Scratch</b>	$0.39 \pm 0.012$	$0.83 \pm 0.027$

The results in Table 4 demonstrate that OmniArch outperforms MPP in parameter estimation tasks, with lower RMSE values indicating more accurate predictions. Models trained

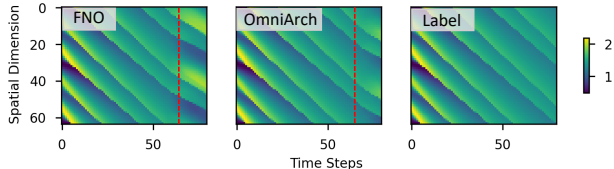


Figure 7: Comparison of Rollout Predictions for 1D Burgers’ Equation. This figure illustrates the predictive performance over steps 80-101 for both the FNO and our OmniArch model, with the post-red dotted line region highlighting the rollout portion.

from scratch yield the highest errors, underscoring the effectiveness of our fine-tuning approach. This evidence supports the notion that OmniArch is not only proficient in forward simulations but also exhibits superior performance in deducing hidden dynamics within complex systems.

### 5.3.5. ROLLOUT PREDICTIONS

We perform rollout experiments to compare the performance of the Fourier Neural Operator (FNO) model and our proposed OmniArch model, as depicted in Figure 7. Our findings indicate that OmniArch demonstrates superior adherence to the underlying physics laws in the initial timesteps, as opposed to merely replicating patterns from other trajectories. This improved fidelity is likely a result of implementing Physics-Informed Reinforcement Learning (PIRL), which isolates the model from the influences of alternate PDE systems, thereby enhancing the model’s ability to generalize physical dynamics.

## 6. Conclusion

In this study, we introduced a pioneering foundation model paradigm for scientific computing, specifically tailored for the resolution of partial differential equations (PDEs). By integrating this model with a novel physics-informed reinforcement learning approach for fine-tuning, we have established new state-of-the-art benchmarks across a comprehensive suite of tasks within the PDEBench framework. Additionally, we investigated the zero-shot learning capabilities of our pre-trained model, uncovering a degree of transferability that mirrors the emergent properties found in large-scale language models. Despite the successes, we recognize the challenges posed by 3D PDE systems to our OmniArch model, which may leave for future research. We envisage that OmniArch will serve as a cornerstone for the development of foundation models in the domain of PDE learning, fostering a significant convergence between scientific machine learning (SciML) and broader deep learning disciplines.



## References

- Allen, K. R., Lopez-Guevara, T., Stachenfeld, K. L., Sanchez-Gonzalez, A., Battaglia, P. W., Hamrick, J. B., and Pfaff, T. Physical design using differentiable learned simulators. *CoRR*, abs/2202.00728, 2022. URL <https://arxiv.org/abs/2202.00728>.
- Beck, C., Hutzenthaler, M., Jentzen, A., and Kuckuck, B. An overview on deep learning-based approximation methods for partial differential equations. *arXiv preprint arXiv:2012.12348*, 2020.
- Bhojanapalli, S., Chakrabarti, A., Glasner, D., Li, D., Unterthiner, T., and Veit, A. Understanding robustness of transformers for image classification. In *2021 IEEE/CVF International Conference on Computer Vision, ICCV 2021, Montreal, QC, Canada, October 10-17, 2021*, pp. 10211–10221. IEEE, 2021. doi: 10.1109/ICCV48922.2021.01007. URL <https://doi.org/10.1109/ICCV48922.2021.01007>.
- Blechschmidt, J. and Ernst, O. G. Three ways to solve partial differential equations with neural networks—a review. *GAMM-Mitteilungen*, 44(2):e202100006, 2021.
- Bommasani, R., Hudson, D. A., Adeli, E., Altman, R., Arora, S., von Arx, S., Bernstein, M. S., Bohg, J., Bosselut, A., Brunskill, E., et al. On the opportunities and risks of foundation models. *arXiv preprint arXiv:2108.07258*, 2021.
- Brown, T., Mann, B., Ryder, N., Subbiah, M., Kaplan, J. D., Dhariwal, P., Neelakantan, A., Shyam, P., Sastry, G., Askell, A., et al. Language models are few-shot learners. *Advances in neural information processing systems*, 33: 1877–1901, 2020.
- Cao, S. Choose a transformer: Fourier or galerkin. *Advances in neural information processing systems*, 34: 24924–24940, 2021.
- Chen, L., Lu, K., Rajeswaran, A., Lee, K., Grover, A., Laskin, M., Abbeel, P., Srinivas, A., and Mordatch, I. Decision transformer: Reinforcement learning via sequence modeling. In Ranzato, M., Beygelzimer, A., Dauphin, Y. N., Liang, P., and Vaughan, J. W. (eds.), *Advances in Neural Information Processing Systems 34: Annual Conference on Neural Information Processing Systems 2021, NeurIPS 2021, December 6-14, 2021, virtual*, pp. 15084–15097, 2021. URL <https://proceedings.neurips.cc/paper/2021/hash/7f489f642a0ddb10272b5c31057f0663-Abstract.html>.
- Cuomo, S., Di Cola, V. S., Giampaolo, F., Rozza, G., Raissi, M., and Piccialli, F. Scientific machine learning through physics-informed neural networks: Where we are and what’s next. *Journal of Scientific Computing*, 92(3):88, 2022.
- Devlin, J., Chang, M.-W., Lee, K., and Toutanova, K. Bert: Pre-training of deep bidirectional transformers for language understanding. *arXiv preprint arXiv:1810.04805*, 2018.
- Du, G., Cao, X., Liang, J., Chen, X., and Zhan, Y. Medical image segmentation based on u-net: A review. *Journal of Imaging Science and Technology*, 2020.
- Geneva, N. and Zabaras, N. Transformers for modeling physical systems. *Neural Networks*, 146:272–289, 2022.
- Golkar, S., Pettee, M., Eickenberg, M., Bietti, A., Cranmer, M. D., Krawezik, G., Lanusse, F., McCabe, M., Ohana, R., Parker, L. H., Blancard, B. R., Tesileanu, T., Cho, K., and Ho, S. xval: A continuous number encoding for large language models. *CoRR*, abs/2310.02989, 2023. doi: 10.48550/ARXIV.2310.02989. URL <https://doi.org/10.48550/arXiv.2310.02989>.
- Guibas, J., Mardani, M., Li, Z., Tao, A., Anandkumar, A., and Catanzaro, B. Efficient token mixing for transformers via adaptive fourier neural operators. In *International Conference on Learning Representations*, 2021.
- Gupta, J. K. and Brandstetter, J. Towards multi-spatiotemporal-scale generalized PDE modeling. *CoRR*, abs/2209.15616, 2022. doi: 10.48550/ARXIV.2209.15616. URL <https://doi.org/10.48550/arXiv.2209.15616>.
- Han, X., Gao, H., Pfaff, T., Wang, J.-X., and Liu, L.-P. Predicting physics in mesh-reduced space with temporal attention. *arXiv preprint arXiv:2201.09113*, 2022.
- Karniadakis, G. E., Kevrekidis, I. G., Lu, L., Perdikaris, P., Wang, S., and Yang, L. Physics-informed machine learning. *Nature Reviews Physics*, 3(6):422–440, 2021.
- Kissas, G., Seidman, J. H., Guilhoto, L. F., Preciado, V. M., Pappas, G. J., and Perdikaris, P. Learning operators with coupled attention. *The Journal of Machine Learning Research*, 23(1):9636–9698, 2022.
- Langley, P. Crafting papers on machine learning. In Langley, P. (ed.), *Proceedings of the 17th International Conference on Machine Learning (ICML 2000)*, pp. 1207–1216, Stanford, CA, 2000. Morgan Kaufmann.
- Li, Z., Kovachki, N., Azizzadenesheli, K., Liu, B., Bhattacharya, K., Stuart, A., and Anandkumar, A. Fourier neural operator for parametric partial differential equations. *arXiv preprint arXiv:2010.08895*, 2020.

- Li, Z., Zheng, H., Kovachki, N., Jin, D., Chen, H., Liu, B., Azizzadenesheli, K., and Anandkumar, A. Physics-informed neural operator for learning partial differential equations. *arXiv preprint arXiv:2111.03794*, 2021.
- Li, Z., Shu, D., and Farimani, A. B. Scalable transformer for PDE surrogate modeling. *CoRR*, abs/2305.17560, 2023. doi: 10.48550/ARXIV.2305.17560. URL <https://doi.org/10.48550/arXiv.2305.17560>.
- Lin, T., Wang, Y., Liu, X., and Qiu, X. A survey of transformers. *AI Open*, 2022.
- Lorsung, C., Li, Z., and Farimani, A. B. Physics informed token transformer. *CoRR*, abs/2305.08757, 2023. doi: 10.48550/ARXIV.2305.08757. URL <https://doi.org/10.48550/arXiv.2305.08757>.
- Lu, L., Jin, P., Pang, G., Zhang, Z., and Karniadakis, G. E. Learning nonlinear operators via deeponet based on the universal approximation theorem of operators. *Nature machine intelligence*, 3(3):218–229, 2021a.
- Lu, L., Meng, X., Mao, Z., and Karniadakis, G. E. Deepxde: A deep learning library for solving differential equations. *SIAM review*, 63(1):208–228, 2021b.
- McCabe, M., Blancard, B. R., Parker, L. H., Ohana, R., Cranmer, M. D., Bietti, A., Eickenberg, M., Golkar, S., Krawezik, G., Lanusse, F., Pettee, M., Tesileanu, T., Cho, K., and Ho, S. Multiple physics pretraining for physical surrogate models. *CoRR*, abs/2310.02994, 2023. doi: 10.48550/ARXIV.2310.02994. URL <https://doi.org/10.48550/arXiv.2310.02994>.
- Mialon, G., Garrido, Q., Lawrence, H., Rehman, D., LeCun, Y., and Kiani, B. T. Self-supervised learning with lie symmetries for partial differential equations. *CoRR*, abs/2307.05432, 2023. doi: 10.48550/ARXIV.2307.05432. URL <https://doi.org/10.48550/arXiv.2307.05432>.
- Oden, J. T. An introduction to the finite element method with applications to nonlinear problems (R. e. white). *SIAM Rev.*, 31(3):512, 1989. doi: 10.1137/1031114. URL <https://doi.org/10.1137/1031114>.
- Pathak, J., Subramanian, S., Harrington, P., Raja, S., Chattopadhyay, A., Mardani, M., Kurth, T., Hall, D., Li, Z., Azizzadenesheli, K., Hassanzadeh, P., Kashinath, K., and Anandkumar, A. Fourcastnet: A global data-driven high-resolution weather model using adaptive fourier neural operators. *CoRR*, abs/2202.11214, 2022. URL <https://arxiv.org/abs/2202.11214>.
- Radford, A., Narasimhan, K., Salimans, T., Sutskever, I., et al. Improving language understanding by generative pre-training. 2018.
- Radford, A., Wu, J., Child, R., Luan, D., Amodei, D., Sutskever, I., et al. Language models are unsupervised multitask learners. *OpenAI blog*, 1(8):9, 2019.
- Radford, A., Kim, J. W., Hallacy, C., Ramesh, A., Goh, G., Agarwal, S., Sastry, G., Askell, A., Mishkin, P., Clark, J., Krueger, G., and Sutskever, I. Learning transferable visual models from natural language supervision. In Meila, M. and Zhang, T. (eds.), *Proceedings of the 38th International Conference on Machine Learning, ICML 2021, 18-24 July 2021, Virtual Event*, volume 139 of *Proceedings of Machine Learning Research*, pp. 8748–8763. PMLR, 2021. URL <http://proceedings.mlr.press/v139/radford21a.html>.
- Raissi, M., Perdikaris, P., and Karniadakis, G. E. Physics-informed neural networks: A deep learning framework for solving forward and inverse problems involving nonlinear partial differential equations. *J. Comput. Phys.*, 378:686–707, 2019. doi: 10.1016/J.JCP.2018.10.045. URL <https://doi.org/10.1016/j.jcp.2018.10.045>.
- Reusch, A., Thiele, M., and Lehner, W. Transformer-encoder and decoder models for questions on math. In Faggioli, G., Ferro, N., Hanbury, A., and Potthast, M. (eds.), *Proceedings of the Working Notes of CLEF 2022 - Conference and Labs of the Evaluation Forum, Bologna, Italy, September 5th - to - 8th, 2022*, volume 3180 of *CEUR Workshop Proceedings*, pp. 119–137. CEUR-WS.org, 2022. URL <https://ceur-ws.org/Vol-3180/paper-07.pdf>.
- Ronneberger, O., Fischer, P., and Brox, T. U-net: Convolutional networks for biomedical image segmentation. In *Medical Image Computing and Computer-Assisted Intervention—MICCAI 2015: 18th International Conference, Munich, Germany, October 5-9, 2015, Proceedings, Part III 18*, pp. 234–241. Springer, 2015.
- Siddique, N., Paheding, S., Elkin, C. P., and Devabhaktuni, V. U-net and its variants for medical image segmentation: A review of theory and applications. *Ieee Access*, 9: 82031–82057, 2021.
- Sirignano, J. and Spiliopoulos, K. Dgm: A deep learning algorithm for solving partial differential equations. *Journal of computational physics*, 375:1339–1364, 2018.
- Subramanian, S., Harrington, P., Keutzer, K., Bhimji, W., Morozov, D., Mahoney, M. W., and Gholami, A. Towards foundation models for scientific machine learning: Characterizing scaling and transfer behavior. *CoRR*, abs/2306.00258, 2023. doi: 10.48550/ARXIV.2306.00258. URL <https://doi.org/10.48550/arXiv.2306.00258>.

- Sun, L., Gao, H., Pan, S., and Wang, J.-X. Surrogate modeling for fluid flows based on physics-constrained deep learning without simulation data. *Computer Methods in Applied Mechanics and Engineering*, 361:112732, 2020.
- Takamoto, M., Praditia, T., Leiteritz, R., MacKinlay, D., Alesiani, F., Pflüger, D., and Niepert, M. Pdebench: An extensive benchmark for scientific machine learning. In Koyejo, S., Mohamed, S., Agarwal, A., Belgrave, D., Cho, K., and Oh, A. (eds.), *Advances in Neural Information Processing Systems 35: Annual Conference on Neural Information Processing Systems 2022, NeurIPS 2022, New Orleans, LA, USA, November 28 - December 9, 2022*, 2022. URL [http://papers.nips.cc/paper\\_files/paper/2022/hash/0a9747136d411fb83f0cf81820d44afb-Abstract-Datasets-and-Benchmarks.html](http://papers.nips.cc/paper_files/paper/2022/hash/0a9747136d411fb83f0cf81820d44afb-Abstract-Datasets-and-Benchmarks.html).
- Touvron, H., Lavril, T., Izacard, G., Martinet, X., Lachaux, M., Lacroix, T., Rozière, B., Goyal, N., Hambro, E., Azhar, F., Rodriguez, A., Joulin, A., Grave, E., and Lample, G. Llama: Open and efficient foundation language models. *CoRR*, abs/2302.13971, 2023a. doi: 10.48550/ARXIV.2302.13971. URL <https://doi.org/10.48550/arXiv.2302.13971>.
- Touvron, H., Martin, L., Stone, K., Albert, P., Almahairi, A., Babaei, Y., Bashlykov, N., Batra, S., Bhargava, P., Bhosale, S., Bikel, D., Blecher, L., Canton-Ferrer, C., Chen, M., Cucurull, G., Esiobu, D., Fernandes, J., Fu, J., Fu, W., Fuller, B., Gao, C., Goswami, V., Goyal, N., Hartshorn, A., Hosseini, S., Hou, R., Inan, H., Kardas, M., Kerkez, V., Khabsa, M., Kloumann, I., Korenev, A., Koura, P. S., Lachaux, M., Lavril, T., Lee, J., Liskovich, D., Lu, Y., Mao, Y., Martinet, X., Mihaylov, T., Mishra, P., Molybog, I., Nie, Y., Poulton, A., Reizenstein, J., Rungta, R., Saladi, K., Schelten, A., Silva, R., Smith, E. M., Subramanian, R., Tan, X. E., Tang, B., Taylor, R., Williams, A., Kuan, J. X., Xu, P., Yan, Z., Zarov, I., Zhang, Y., Fan, A., Kambadur, M., Narang, S., Rodriguez, A., Stojnic, R., Edunov, S., and Scialom, T. Llama 2: Open foundation and fine-tuned chat models. *CoRR*, abs/2307.09288, 2023b. doi: 10.48550/ARXIV.2307.09288. URL <https://doi.org/10.48550/arXiv.2307.09288>.
- Tran, A., Mathews, A., Xie, L., and Ong, C. S. Factorized fourier neural operators. *arXiv preprint arXiv:2111.13802*, 2021.
- Vaswani, A., Shazeer, N., Parmar, N., Uszkoreit, J., Jones, L., Gomez, A. N., Kaiser, Ł., and Polosukhin, I. Attention is all you need. *Advances in neural information processing systems*, 30, 2017.
- Wang, S., Wang, H., and Perdikaris, P. Learning the solution operator of parametric partial differential equations with physics-informed deepoanets. *Science advances*, 7(40): eabi8605, 2021.
- Wei, J., Tay, Y., Bommasani, R., Raffel, C., Zoph, B., Borgeaud, S., Yogatama, D., Bosma, M., Zhou, D., Metzler, D., Chi, E. H., Hashimoto, T., Vinyals, O., Liang, P., Dean, J., and Fedus, W. Emergent abilities of large language models. *Trans. Mach. Learn. Res.*, 2022, 2022. URL <https://openreview.net/forum?id=yzkSU5zdwD>.
- Wen, Q., Zhou, T., Zhang, C., Chen, W., Ma, Z., Yan, J., and Sun, L. Transformers in time series: A survey. *arXiv preprint arXiv:2202.07125*, 2022.
- Yang, L., Liu, S., Meng, T., and Osher, S. J. In-context operator learning with data prompts for differential equation problems. *Proceedings of the National Academy of Sciences*, 120(39):e2310142120, 2023a.
- Yang, L., Meng, T., Liu, S., and Osher, S. J. Prompting in-context operator learning with sensor data, equations, and natural language. *CoRR*, abs/2308.05061, 2023b. doi: 10.48550/ARXIV.2308.05061. URL <https://doi.org/10.48550/arXiv.2308.05061>.
- Zhou, C., Li, Q., Li, C., Yu, J., Liu, Y., Wang, G., Zhang, K., Ji, C., Yan, Q., He, L., et al. A comprehensive survey on pretrained foundation models: A history from bert to chatgpt. *arXiv preprint arXiv:2302.09419*, 2023.

## A. Dataset Details

### A.1. Dataset For Zero-shot Learning

We choose three test datasets from PDEBench to validate zero-shot ability of our model. They all belong to two-dimensional compressible Navier-Stokes equations, but are different fluid phenomena that exhibit distinct physical mechanisms and characteristics. Brief introductions and details of the datasets are as follows:

- **OTVortex:** The Orszag-Tang Vortex system is a compressible flow problem that generates highly complex vortex structures through the careful selection of initial conditions. The dataset includes one exsample, which is a  $1024 \times 1024$  resolution physical field evolved over 101 time steps with a time interval of 0.01.
- **2D Shock:** Shock waves are characterized by abrupt changes in flow properties resulting from sudden discontinuities in fluid flow, such as rapid changes in pressure, temperature, and density. The dataset includes one exsample, which is also a  $1024 \times 1024$  resolution physical field evolved over 101 time steps with a time interval of 0.01.
- **2D KH:** The Kelvin-Helmholtz instability is a fluid instability that occurs at the interface between two fluid layers with different velocities or densities. This dataset consists of seven exsamples generated based on different parameters  $M$ ,  $dk$ , and  $Re$ . Each is a  $1024 \times 1024$  resolution physical field evolved over 51 time steps with a time interval of 0.1. We conducted experiments on all samples and averaged the results.

### A.2. Examples of Generated PDES

#### A.2.1. BURGERS 1D

- Original form:

$$\partial_t u(t, x) + \partial_x(u^2(t, x)/2) = \nu/\pi \partial_{xx} u(t, x), \quad x \in (0, 1), t \in (0, 2],$$

$$u(0, x) = u_0(x), \quad x \in (0, 1),$$

- After augmented:

$$0.77 \int \left( \frac{\partial}{\partial t} v(t, x) + \frac{\partial}{\partial x} \frac{v^2(t, x)}{2} \right) dt = \frac{0.77\nu \int \frac{\partial^2}{\partial x^2} v(t, x) dt}{\pi}$$

$$0.73tv(0, x) = 0.73tv_0(x)$$

- Explanation: We replace  $u$  with  $v$  and  $\partial_t$  with  $\frac{\partial}{\partial t}$ . We integrate and multiply some factors on both sides of the equation at the same time.

#### A.2.2. ADVECTION

- Original form:

$$\partial_t u(t, x) + \beta \partial_x u(t, x) = 0, \quad x \in (0, 1), t \in (0, 2],$$

$$u(0, x) = u_0(x), \quad x \in (0, 1),$$

- After augmented:

$$1.45 \int \left( c \frac{\partial}{\partial x} A(t, x) + \frac{\partial}{\partial t} A(t, x) \right) dt = 0$$

$$A(0, x) = A_0(x)$$

- Explanation: We replace  $u$  with  $A$ ,  $\partial_t$ ,  $\partial_x$  with  $\frac{\partial}{\partial t}$ ,  $\frac{\partial}{\partial x}$ , and  $\beta$  with  $c$ . We integrate and multiply some factors on both sides of the equation at the same time.



## A.2.3. CFD 1D

- Original form:

$$\begin{aligned}\partial_t \rho + \nabla \cdot (\rho \mathbf{v}) &= 0, \\ \rho(\partial_t \mathbf{v} + \mathbf{v} \cdot \nabla \mathbf{v}) &= -\nabla p + \eta \Delta \mathbf{v} + (\zeta + \eta/3) \nabla(\nabla \cdot \mathbf{v}), \\ \partial_t \left[ \epsilon + \frac{\rho v^2}{2} \right] + \nabla \cdot \left[ \left( \epsilon + p + \frac{\rho v^2}{2} \right) \mathbf{v} - \mathbf{v} \cdot \sigma' \right] &= 0,\end{aligned}$$

- After augmented:

$$\varrho(t, x) \frac{\partial}{\partial x} \mathbf{w}(t, x) + \frac{\partial}{\partial t} \varrho(t, x) = 0$$

$$0.61 \left( \mathbf{w}(t, x) \frac{\partial}{\partial x} \mathbf{w}(t, x) + \frac{\partial}{\partial t} \mathbf{w}(t, x) \right) \varrho(t, x) = 0.61 \eta \frac{\partial^2}{\partial x^2} \mathbf{w}(t, x) + 0.61 \left( \chi + \frac{\eta}{3} \right) \frac{\partial^2}{\partial x^2} \mathbf{w}(t, x) - 0.61 \frac{\partial}{\partial x} p(t, x)$$

$$\int \left( \frac{\partial}{\partial t} \left( \epsilon + \frac{\mathbf{w}^2(t, x) \varrho(t, x)}{2} \right) + \frac{\partial}{\partial x} \left( -\tau \mathbf{w}(t, x) + \left( \epsilon + \frac{\mathbf{w}^2(t, x) \varrho(t, x)}{2} + p(t, x) \right) \mathbf{w}(t, x) \right) \right) dt = 0$$

- Explanation: We replaced many symbols, such as replacing  $\nabla$  with  $\partial_t$  and  $\Delta$  with  $\frac{\partial^2}{\partial x^2}$ . We integrate and multiply some factors on both sides of the equation at the same time. We also swapped the order of some items, such as  $\zeta + \eta/3$ .

## B. Training Details

In our training process, the following strategies or decisions were made:

- **Pre/Post Norm:** Pre-norm
- **Norm Type:** RMS Norm Type
- **Architecture:** Decoder-Only
- **Attention-Type:** Multi-scaled Attention
- **Position Embedding:** RoPE
- **Casual Masking:** True- We only evaluate the loss on the T + 1 physical fields prediction.
- **Hidden Size:** 1024
- **initializer\_range:** 0.02
- **intermediate\_size:** 4096
- **num\_attention\_heads:** 16
- **num\_attention\_heads:** 16

**Software.** We mainly used Pytorch and pytorch-lightning for most of the main development and experiments. We also use MindSpore for some inference tasks.

**Hardware.** The main development and experiments were conducted on NVIDIA A800-80GiB GPUs.